Systematically derived one-step kinetics for hydrogen-air gas-turbine combustion

Jaime Carpio[a], Brandon Li[b], Daniel Fernández-Galisteo[c], Antonio L. Sánchez[b], Forman A. Williams[b]

[a]*Dept. Ingeniería Energética, E.T.S.I. Industriales, Universidad Politécnica de Madrid, Madrid, 28006, Spain*
[b]*Dept. Mechanical and Aerospace Engineering, University of California San Diego, La Jolla CA 92093-0411, USA*
[c]*Department of Energy, Centro de Investigaciones Energéticas, Medioambientales y Tecnológicas, Madrid, 28040 Spain*

Abstract

A previously derived one-step reduced chemical-kinetic mechanism, describing hydrogen flames under near-limit conditions involving peak temperature not far from the crossover temperature, is used in computations of hydrogen-air flamelets at elevated pressures typical of gas-turbine combustion. Besides freely propagating laminar deflagrations with compositions spanning the whole range of flammability conditions, the calculations address strained premixed and nonpremixed flames as well as partially premixed propagating fronts. The comparisons with results of detailed-chemistry computations reveal that, for most purposes, the one-step mechanism provides sufficiently accurate predictions of burning rates under all conditions of interest for gas-turbine combustion. The reduced-chemistry model, featuring an explicit analytic expression for the hydrogen oxidation rate in terms of the local temperature and the O_2, H_2, and H_2O concentrations, can be easily implemented in numerical codes, thereby facilitating future numerical analyses based on direct-numerical and large-eddy simulations.

Keywords: Hydrogen, high-pressure combustion, gas turbines

1. Introduction

The continued necessity of providing for large-scale on-demand power generation and propulsion, in the face of mushrooming environmental needs for reducing emissions of carbon dioxide and dependence on fossil fuels, focuses attention on gas turbines as essential components of any system [1]. Because of their environmental and economic benefits, hydrogen-fueled gas turbines are bound to play an important role in foreseeable carbon-free energy-production scenarios [2]. Manufactures are moving from systems fueled by natural

Email address: als@ucsd.edu (Antonio L. Sanchez)

gas to new designs involving hydrogen addition to carbon-containing or carbon-free fuels, such as ammonia, or simply using only hydrogen. Experimental and computational investigations have shown, however, that hydrogen affects gas-turbine combustion processes substantially [3]. A critical need therefore exists for simple and efficient means for describing the chemical kinetics of hydrogen combustion sufficiently accurately under gas-turbine conditions.

Different approaches have been pursued in deriving simplified kinetics for hydrogen combustion. A single overall step has been derived on the basis of detailed-chemistry flame computations by selecting the Arrhenius rate parameters from a least square fit of the heat release profile [4]. Similar one-step descriptions targeting specific combustion conditions have been shown to be useful in addressing particular problems, including deflagration-to-detonation transition [5] and supersonic combustion [6]. The accuracy of all of these ad hoc descriptions degrades rapidly outside the narrow ranges of temperature, pressure, and composition for which they were originally developed, so that their utility is limited. Reduced mechanisms that are systematically derived from first principles are more useful in that respect. Simplifications can be achieved through introduction of steady-state approximations for chemical intermediates that exhibit negligibly small transport rates, resulting in reduced mechanisms involving a few overall steps with global reaction rates that are evaluated from those of the elementary reactions [7]. For example, for hydrogen a two-step mechanism with H as the only intermediate not following steady state has been shown to describe with sufficient accuracy flame propagation under a wide range of conditions [8]. More complicated descriptions apply in autoignition processes, for which either HO_2 (above the second explosion limit) or H_2O_2 (below the second explosion limit) are found to be out of steady state [9]. The steady-state assumption for OH loses accuracy when autoignition takes place in nonpremixed environments, including laminar mixing layers [10] and turbulent jets [11], for which a minimum of three global steps are needed. Following these previous ideas, the current paper exploits steady-state simplifications applying for hydrogen-air combustion at high pressure, under which conditions a one-step mechanism suffices to describe many aspects of the combustion process, as explained below.

Typical gas-turbine combustion conditions include elevated pressures in the range $10\text{atm} < p < 50\text{atm}$, resulting in post-compression temperatures on the order of 700 K. To avoid large NO emissions, the accompanying peak temperatures in the combustor must be limited—by means of dilution through exhaust-gas recirculation or by use of extremely fuel-lean mixtures—to values not exceeding significantly $T_{max} \sim 2,000$ K. The existing high pressures promote radical recombination through three-body recombination reactions in such a way that the rate of radical branching and that of radical recombination do not differ by a large amount in the thin hot reaction layers where the fuel is oxidized, so that the key intermediates H, O, OH, and HO_2 maintain steady states there, their transport rates playing minor roles in determining the local heat-release rate. Under those conditions, hydrogen oxidation effectively proceeds according to the global reaction

$$2H_2 + O_2 \rightarrow 2H_2O, \tag{1}$$

with an overall rate that can be expressed in closed analytic form in terms of the local

temperature and the O_2, H_2, and H_2O concentrations [12], thereby providing an attractive simple chemistry description. The level of accuracy to be expected when using this one-step chemistry in gas-turbine combustion simulations is to be assessed below through flamelet computations involving three canonical configurations, namely, steady planar deflagrations, counterflow premixed and nonpremixed flames, and two-dimensional triple flames.

2. Description of the one-step chemistry

Under gas-turbine combustion conditions, hydrogen oxidation is controlled by nine elementary steps [7], namely, the reversible shuffle reactions $H+O_2 \overset{1}{\rightleftharpoons} OH+O$, $H_2+O \overset{2}{\rightleftharpoons} OH+H$, and $H_2+OH \overset{3}{\rightleftharpoons} H_2O+H$, the irreversible three-body reactions $H+O_2+M \overset{4f}{\rightarrow} HO_2+M$, $H+OH+M \overset{8f}{\rightarrow} H_2O+M$ and $H+H+M \overset{9f}{\rightarrow} H_2+M$, and the irreversible hydroperoxyl-consumption reactions $HO_2+H \overset{5f}{\rightarrow} OH+OH$, $HO_2+H \overset{6f}{\rightarrow} H_2+O_2$, and $HO_2+OH \overset{7f}{\rightarrow} H_2O+O_2$. Corresponding reaction-rate constants k can be found in [13], including separate expressions for the rate parameters of the forward (f) and backward (b) reactions.

As shown in [12], when all hydrogen-oxygen radicals obey a steady-state approximation, the combined effect of all nine elementary reactions can be represented by the global reaction (1) whose rate ω (moles per unit volume per unit time) is given by the sum of the elementary rates of reactions $4f$, $8f$, and $9f$, thereby giving

$$\omega = k_{4f} C_{\mathrm{M}_4} C_{\mathrm{O}_2} C_{\mathrm{H}} + k_{8f} C_{\mathrm{M}_8} C_{\mathrm{OH}} C_{\mathrm{H}} + k_{9f} C_{\mathrm{M}_9} C_{\mathrm{H}}^2, \tag{2}$$

where C_i and C_{M_j} denote the concentration of species i and the effective third-body concentration, the latter evaluated for each reaction $j = (4f, 8f, 9f)$ with account taken of its specific chaperon efficiencies. The rate (2) depends on the local values of the H and OH concentrations, which can be determined by algebraic manipulation of the steady-state equations for H, OH, O, and HO_2 to yield [12]

$$C_{\mathrm{H}} = \frac{1}{GH} \frac{k_{2f} k_{3f} C_{\mathrm{H}_2}^2}{k_{1b} k_{4f} C_{\mathrm{M}_4} C_{\mathrm{O}_2}} \left(\frac{k_{1f}}{\alpha k_{4f} C_{\mathrm{M}_4}} - 1 \right), \tag{3}$$

and

$$C_{\mathrm{OH}} = \frac{1}{H} \frac{k_{2f} C_{\mathrm{H}_2}}{k_{1b}} \left(\frac{k_{1f}}{\alpha k_{4f} C_{\mathrm{M}_4}} - 1 \right), \tag{4}$$

involving the three dimensionless functions G, H, and

$$\alpha = \frac{k_{6f} f/(k_{5f} + k_{6f}) + G}{f + G}, \tag{5}$$

with

$$f = \frac{k_{5f} + k_{6f}}{k_{7f}} \frac{k_{3f}}{k_{4f} C_{\mathrm{M}_4}} \frac{C_{\mathrm{H}_2}}{C_{\mathrm{O}_2}} \tag{6}$$

(expressions for the order-unity functions G and H are considerably more involved and can be found in [12]). The resulting overall rate depends on the temperature and on the concentrations of H_2, O_2, and H_2O, the last dependence entering in the function G through

the backward reaction $H_2O+H \overset{3b}{\rightarrow} H_2+OH$ [12]. Although almost impossibly complex algebraically, it is exceedingly simple computationally to evaluate ω directly from (2).

As can be seen from the formulas above, the radical concentrations (3) and (4) contain a cutoff factor $(k_{1f} - \alpha k_{4f} C_{M_4})$ that becomes zero as the temperature T reaches the crossover value T_c at which the rate of radical production matches the rate of radical recombination, as defined by the condition

$$k_{1f} = \alpha k_{4f} C_{M_4}. \tag{7}$$

In the present approximation, all radical concentrations vanish for $T < T_c$ and, correspondingly, the reaction rate (2) must be set equal to zero. Because of its key role in hydrogen combustion, it is of interest to review briefly the dependence of T_c on the combustion conditions. Besides the well-known increase with increasing pressure p, resulting from the linear proportionality $C_{M_4} \propto p$, the crossover temperature determined from (7) exhibits a dependence on the mixture composition, partly because H_2 and H_2O have increased chaperon efficiencies (i.e. 16 for H_2O and 2.5 for H_2 in reaction $4f$) compared with nitrogen and other species and partly through the factor α defined in (5).

To understand the latter dependence, which enters mainly through the function f defined in (6), it is important to note that the three-body reaction $H+O_2+M \overset{4f}{\rightarrow} HO_2+M$ is chain-carrying, in that in eliminating one hydrogen atom it creates one hydroperoxyl radical, so that the total number of radicals is not altered. To determine the net recombination efficiency of reaction $4f$ one must therefore investigate the subsequent consumption of HO_2 through collisions with H and OH radicals. In very lean mixtures the prevailing consumption route involves collisions with OH through reaction $HO_2+OH \overset{7f}{\rightarrow} H_2O+O_2$, which is chain-terminating, resulting in a value of $\alpha = 1$, as can be seen by taking the limit $f \ll 1$ in (5). The associated overall rate takes in the case the simplified form

$$\omega = \left(\frac{k_{1f}}{k_{4f} C_{M_4}} - 1 \right) \frac{k_{2f} k_{3f}/k_{1b}}{1 + \frac{k_{3b} C_{H_2O}}{k_{4f} C_{M_4} C_{O_2}}} C_{H_2}^2 \tag{8}$$

with the crossover temperature, determined with $\alpha = 1$ from $k_{1f} = k_{4f} C_{M_4}$, taking the values $T_c \simeq 1000$ K at $p = 1$ atm and $T_c \simeq 1800$ K at $p = 40$ atm.

By way of contrast, in very rich mixtures, corresponding to the opposite limit $f \gg 1$, the concentration of H is much larger than that of OH, with the result that HO_2 consumption occurs instead through reactions $HO_2+H \overset{5f}{\rightarrow} OH+OH$ (chain-carrying) and $HO_2+H \overset{6f}{\rightarrow} H_2+O_2$ (chain-terminating). Since $k_{6f}/(k_{5f} + k_{6f}) \simeq 1/6$ regardless of the temperature, it turns out from (5) that only one sixth of the collisions involving HO_2 effectively removes radicals, a fact clearly reflected in the limiting value $\alpha \simeq k_{6f}/(k_{5f} + k_{6f}) \simeq 1/6$ of α for $f \gg 1$. Since the effective rate of radical removal through $H+O_2+M \overset{4f}{\rightarrow} HO_2+M$ is diminished, the resulting crossover temperature is significantly lower, as can be seen by evaluating $k_{1f} = (1/6) k_{4f} C_{M_4}$ to give $T_c \simeq 700$ K at $p = 1$ atm and $T_c \simeq 1300$ K at $p = 40$ atm. It then can be seen by using (3) in the dominant leading term in (2) that in this limiting case

the overall rate takes the simplified form

$$\omega = \left(\frac{k_{1f}}{k_{4f} C_{\mathrm{M}_4}} - \frac{k_{6f}}{k_{5f} + k_{6f}} \right) \frac{(k_{4f} C_{\mathrm{M}_4})^2}{\frac{k_{3b} C_{\mathrm{H_2O}}}{k_{3f} C_{\mathrm{H_2}}} k_{8f} C_{\mathrm{M}_8} + k_{9f} C_{\mathrm{M}_9}} C_{\mathrm{O}_2}^2, \tag{9}$$

which has been used to analyze pulsating deflagration propagation in fuel-rich hydrogen-air mixtures [14].

It can be expected that the steady-state approximation holds under conditions such that the temperature difference $T_{max} - T_c$ is limited to a few hundred kelvin, so that the resulting radical transport rate (the difference between the production rate by radical branching and the consumption rate by radical recombination) remains significantly smaller than the chemical rates. This condition is satisfied near the lean flammability limit [15, 16], as well as for sufficiently rich mixtures, with the mechanism describing accurately the dynamics of pulsating flames [14]. In general, radical steady states are favored by low values of the peak temperatures, as occurs when the mixture is diluted with combustion products, or by high values of the crossover temperature, as occurs at high pressure. The computations of high-pressure hydrogen-air flamelets shown below, including freely propagating deflagrations, counterflow diffusion flames and triple flames propagating in strained mixing layers, suggest that the steady-state approximation is sufficiently accurate under conditions of interest for gas-turbine combustion, for which the simple one-step chemistry described above becomes applicable.

3. Comparisons of one-step and detailed-chemistry predictions

To test the accuracy of the one-step mechanism, results of different flamelet configurations involving H_2-O_2-N_2 mixtures are compared with detailed-chemistry computations using the 20-step San Diego mechanism [17] in Figs. 2-5. We begin by investigating steady planar deflagrations, first reviewing the dependence of the accuracies of flame-structure approximations on pressure.

3.1. Steady planar deflagrations

Figure 1 shows the variation with pressure of the flame propagation velocity S_L for a lean H_2-air mixture with equivalence ratio $\phi = 0.7$ and initial temperature $T_u = 300$ K as obtained with detailed chemistry (solid curve) and reduced chemistry (dashed curve). For illustrative purposes, the equivalence ratio here was selected to lie in the vicinity of the values most often encountered in practice, the initial temperature approximating normal room temperature, but the general conclusions to be drawn concerning pressure dependences apply at essentially all conditions. The accompanying upper panel shows the variation of the corresponding adiabatic flame temperature T_b and crossover temperature T_c, the latter determined from (7) using the equilibrium composition. The computations employ a multicomponent transport description including thermal diffusion [18, 19].

To investigate the applicability of the steady-state assumption, the figure includes insets showing the rates of H-atom production, consumption and transport across the flame for

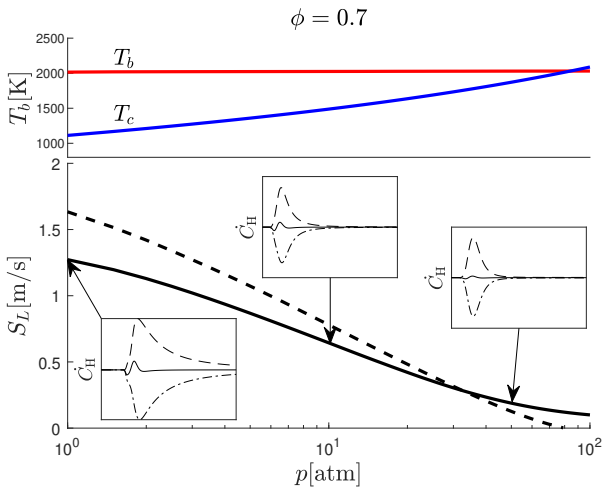

Figure 1: The variation with pressure of the burning rate S_L corresponding to lean H_2-air mixtures with equivalence ratio $\phi = 0.7$ and initial temperature $T_u = 300$ K as obtained with detailed chemistry (solid curve) and with the one-step reduced mechanism (dashed curve), with the insets showing the variation of the rates of production (dashed curves), consumption (dot-dashed curves), and transport (solid curves) across the flame for three different pressures $p = (1, 10, 50)$ atm. The upper plot represents the variation of the adiabatic flame temperature T_b and of the crossover temperature T_c, the latter evaluated from (7).

three selected pressures, with the flame propagating leftward. For $p = 1$ atm, the H-atom transport rate is seen to be comparable to its production and consumption rates at the onset of reaction near the left boundary, indicating that a steady-state assumption for H atoms is inaccurate for these conditions. The relative magnitude of the transport rate diminishes as the crossover temperature approaches the adiabatic flame temperature for increasing pressure, as can be seen in the plots for $p = 10$ atm and $p = 50$ atm. The results indicate that the steady-state approximation becomes reasonably accurate for all radicals at these intermediate high pressures 10 atm $< p <$ 50 atm, typical of gas-turbine combustion, with the consequence that the one-step reduced kinetics, which does not perform well at ambient pressure, provides a good description of the resulting burning rate, as seen in the figure. The flame velocity computed with the one-step mechanism vanishes as T_c approaches T_b, in this case for $p \simeq 80$ atm, as expected from (3) and (4). At these high pressures, radical regeneration by the hydrogen peroxide decomposition reaction H_2O_2+M $\rightarrow$ OH+OH+M opens up an alternative chain-branching path that enables fuel oxidation to proceed at a very low rate. Since the starting nine-step skeletal mechanism used in our development does not include hydrogen peroxide, these slow flames, of limited interest for practical purposes in combustion applications, cannot be described with the one-step mechanism.

Figure 2 shows the variation with equivalence ratio ϕ of the corresponding flame propagation velocity S_L at two different pressures. The figure also displays the variation with ϕ of the adiabatic flame temperature T_b, which is the peak temperature across the flame in the absence of heat losses, along with an indication of the corresponding crossover temperature T_c determined from the condition (7) for $\alpha = 1$ (lean limit) and $\alpha = 1/6$ (rich limit), with the

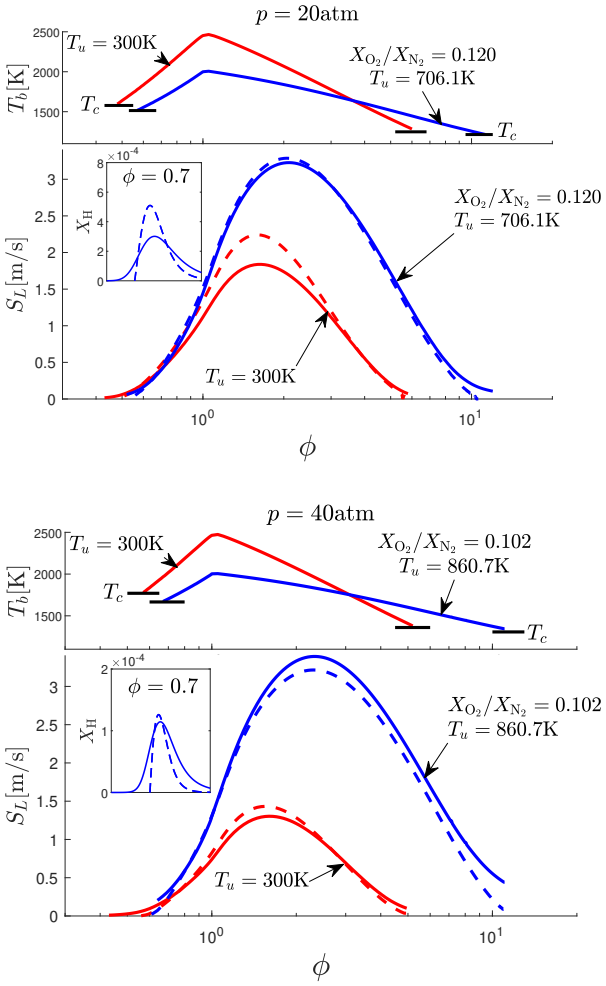

Figure 2: The variation with equivalence ratio of the burning rate S_L corresponding to H_2-air mixtures with initial temperature $T_u = 300$ K (red curves) and to preheated H_2-O_2-N_2 mixtures (blue curves) with oxygen-nitrogen mole-fraction ratio $X_{O_2}/X_{N_2} = 0.120$ ($p = 20$ atm) and $X_{O_2}/X_{N_2} = 0.102$ ($p = 40$ atm) as obtained with detailed chemistry (solid curve) and with the one-step reduced mechanism (dashed curve). The insets show the corresponding H-atom mole fractions across the flame for a preheated mixture with $\phi = 0.7$. The plots also include the associated variation of the adiabatic flame temperature T_b, with indication of the crossover temperature T_c corresponding to the lean and rich limits for each case.

chaperon efficiencies computed with the composition at equilibrium. Besides results corresponding to hydrogen-air mixtures with initial temperature $T_u = 300$ K, represented by red curves, consideration is given to preheated mixtures, with the initial temperature computed from the isentropic compression relation $T_u = 300p^{(\gamma-1)/\gamma}$ using $\gamma = 1.4$ for the specific-heat ratio, with T_u and p expressed in kelvin and atmospheres, respectively, yielding $T_u = 706.1$ K for $p = 20$ atm and $T_u = 860.7$ K for $p = 40$ atm. To represent the effect of exhaust-gas recirculation, needed to limit the peak temperature in these preheated cases, the mixture is diluted with nitrogen, with the initial oxygen-to-nitrogen mole-fraction ratio X_{O_2}/X_{N_2} lowered from the value $(X_{O_2}/X_{N_2})_{AIR} = 0.266$ corresponding to air to give an adiabatic flame temperature $T_b = 2000$ K for $\phi = 1$. The resulting values, $X_{O_2}/X_{N_2} = 0.120$ for $p = 20$ atm and $X_{O_2}/X_{N_2} = 0.102$ for $p = 40$ atm, are then used together with $\phi = 2X_{H_2}/X_{O_2}$ to determine the initial composition for the computations represented by the blue curves in Fig. 2.

The results in Fig. 2 reveal that the one-step kinetics predicts with reasonable accuracy the burning rate for all conditions explored in the figure, including mixtures where the peak temperature departs significantly from T_c. The observed relative differences in flame-propagation velocities determined with the reduced and detailed chemistries $(S_{L_{RED}} - S_{L_{DET}})/S_{L_{DET}}$ are seen to remain below about 10% for $T_{max} - T_c \lesssim 500$ K.

To further test the accuracy of the quasi-steady approximation, the insets in Fig. 2 compare the H-atom mole fraction X_H across the flame obtained with detailed chemistry (solid curves) with that corresponding to the reduced chemistry (dashed curves), the latter computed by evaluating (3) with the concentrations of H_2, O_2, and H_2O and temperature determined with the one-step computations. As can be seen, the agreement is reasonably good, especially for $p = 40$ atm, with the main departures occurring at crossover, where the reduced kinetics predicts H atoms to disappear abruptly, because of the cutoff factor present in (3), thereby giving a profile with a discontinuous slope, whereas the detailed-chemistry H-atom profile is smoothed out by diffusive transport.

The mole fraction of H, as well as those of the other intermediates, are extremely small, so that they give a negligible contribution to the elemental balances of hydrogen and oxygen. As a result, the corresponding profiles of reactants and water vapor computed with the reduced and detailed kinetics (not shown in the insets) are nearly indistinguishable. Clearly, higher-order corrections accounting for the mass of radicals in the elemental balances, which have been shown to improve reduced-chemistry predictions of hydrogen-air flames at atmospheric pressure [8], are not needed for describing flames under gas-turbine combustion conditions.

As previously indicated in Fig. 1, in the one-step approximation the flame propagation velocity vanishes when the adiabatic flame temperature T_b reaches T_c, because ω becomes zero all across the flame. Therefore, the condition $T_b = T_c$ effectively introduces lean and rich chemical-kinetic flammability limits ϕ_l and ϕ_r. Since heat losses (e.g. by radiation) are not included in the computations, the curves representing detailed-chemistry results do not show these neatly defined flammability limits. Instead, at temperatures below crossover, corresponding to equivalence ratios $\phi < \phi_l$ and $\phi > \phi_r$, reactions involving H_2O_2, which are not included in the one-step mechanism because they are largely unimportant for describing flame propagation at high temperature, enable a slow path of hydrogen oxidation [7] to be

followed, although radiant heat loss would soon extinguish that chemistry. The resulting nonzero values of S_L are, in addition, too small to be of practical interest, especially beyond the lean limit (i.e. $\phi < \phi_l$), where the predicted velocity is just a few centimeters per second. The detailed chemistry predicts somewhat larger values of S_L in diluted mixtures with $\phi > \phi_r \simeq 10$. The description of flame propagation under these extremely fuel-rich conditions must account, in particular, for hydroperoxyl recombination through $H_2 + HO_2 \rightarrow H_2O_2 + H$, but the associated analysis is not pursued here because this regime is of limited interest in gas-turbine applications.

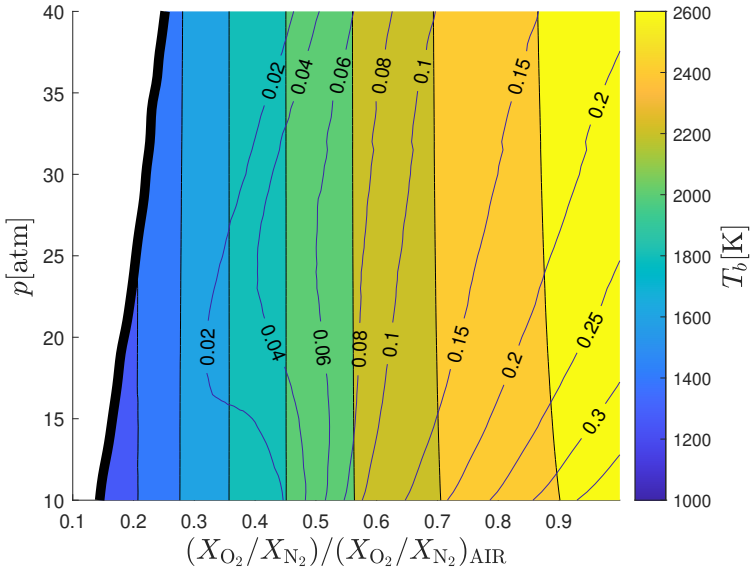

Figure 3: The variation with pressure and dilution of the relative error $(S_{L_{\rm RED}} - S_{L_{\rm DET}})/S_{L_{\rm DET}}$ in computations of stoichiometric laminar-flame propagation velocities for an initial temperature $T_u = 700$ K. Color contours are used to indicate the accompanying variation of the adiabatic flame temperature.

To further assess the accuracy of the one-step kinetics in combustion scenarios involving high-pressure diluted flames, of interest in gas-turbine combustion, additional results of flame-propagation computations pertaining to stoichiometric H_2-air mixtures diluted with nitrogen are addressed in the diagram shown in Fig. 3. The computations correspond to preheated mixtures with $T_u = 700$ K for pressures in the range 10 atm $< p <$ 40 atm. At each pressure, the mixture oxygen-to-nitrogen ratio X_{O_2}/X_{N_2} is varied from the value $(X_{O_2}/X_{N_2})_{AIR} = 0.266$ corresponding to air down to the value that yields $T_b = T_c$, beyond which the stoichiometric mixture is no longer flammable according to the one-step chemistry. Isocontours of constant relative error $(S_{L_{\rm RED}} - S_{L_{\rm DET}})/S_{L_{\rm DET}}$ are plotted along with color contours of peak temperature T_b. As can be seen, over the entire range of pressures considered in the figure, errors between about 2 % and 10 % can be expected in gas turbines operating at peak temperatures in the range 1600 K $\lesssim T_b \lesssim$ 2200 K, those being the conditions most often found in applications.

3.2. Counterflow flames

The performance of the mechanism in connection with strained flamelets was investigated in computations of one-dimensional premixed and nonpremixed flames in planar counterflow mixing layers at $p = 25$ atm and $p = 50$ atm (see [20] for details of the formulation and associated simplifications). Results of twin premixed flames generated in configurations with identical opposed streams at $T = 300$ K are shown in the upper plots of Fig. 4 for H_2-O_2-N_2 mixtures with $\phi = 0.7$ and three different levels of dilution, including undiluted H_2-air mixtures (i.e. $X_{O_2}/X_{N_2} = 0.266$). These conditions were selected to correspond to those in Fig. 1. The plots represent the variation of the peak temperature over a wide range of strain rates A (with A denoting the value in the outer potential air stream) extending over about two orders of magnitude up to extinction. The curves show the expected superadiabatic temperatures at intermediate values of the strain rate, a result attributable to effects of preferential diffusion of hydrogen [21]. For H_2-air mixtures, the performance of the one-step mechanism is not satisfactory, especially near extinction, as may be seen in burning-velocity plots (not shown) because the resulting peak temperatures are far above the corresponding crossover values at these pressures, shown in the upper panel of Fig. 1. Much better agreement is found for diluted conditions that lower the peak temperature to values typically found in applications, for which the reduced chemistry describes with sufficient accuracy the flame response to strain, including the critical value of the strain rate at extinction.

The intermediate and lower plots of Fig. 4 show results of diffusion flames involving a stream of air counterflowing against a stream of hydrogen diluted with nitrogen, both feed streams at $T = 300$ K, with $X_{H_2,0}$ denoting the fuel mole fraction in its feed stream. Besides intermediate panels representing the variation with strain rate of the peak temperature, the figure shows in the accompanying lower panels the associated burning rate per unit flame area $\dot{m}_{H_2}$ (mols cm^{-2} s^{-1}) obtained by integrating the fuel consumption rate across the mixing layer. In the one-step computations, the fuel consumption rate is simply 2ω, with ω given in (9), whereas in the detailed computations the evaluation accounts for the separate contributions of the five elementary reactions of the 20-step mechanism that involve H_2 molecules, namely, $H_2+O \overset{2}{\rightleftharpoons} OH+H$, $H_2+OH \overset{3}{\rightleftharpoons} H_2O+H$, $HO_2+H \overset{6}{\rightleftharpoons} H_2+O_2$, $H+H+M \overset{9}{\rightleftharpoons} H_2+M$, and $H_2 + HO_2 \rightleftharpoons H_2O_2 + H$.

It can be seen from the intermediate and lower plots that the one-step mechanism reproduces the expected decrease of peak temperature and associated increase of burning rate with increasing strain rate, until a maximum value of the strain rate A_{ext} is reached at which extinction is seen to occur. Since the computations employ a time-marching scheme, which is advanced in time until a steady solution is attained, only the upper branch of the S-shape curve of the peak temperature as a function of a Damkholer number based on the strain rate can be described. The agreement between the one-step and the detailed-chemistry computations is excellent for the largest dilution considered ($X_{H_2,0} = 0.25$), especially for $p = 50$ atm, for which the departures in the predicted peak temperatures are only about 10K and the error in the critical strain rate at extinction is only about 10%. The agreement deteriorates with decreasing dilution, as the peak temperature in the reaction region departs

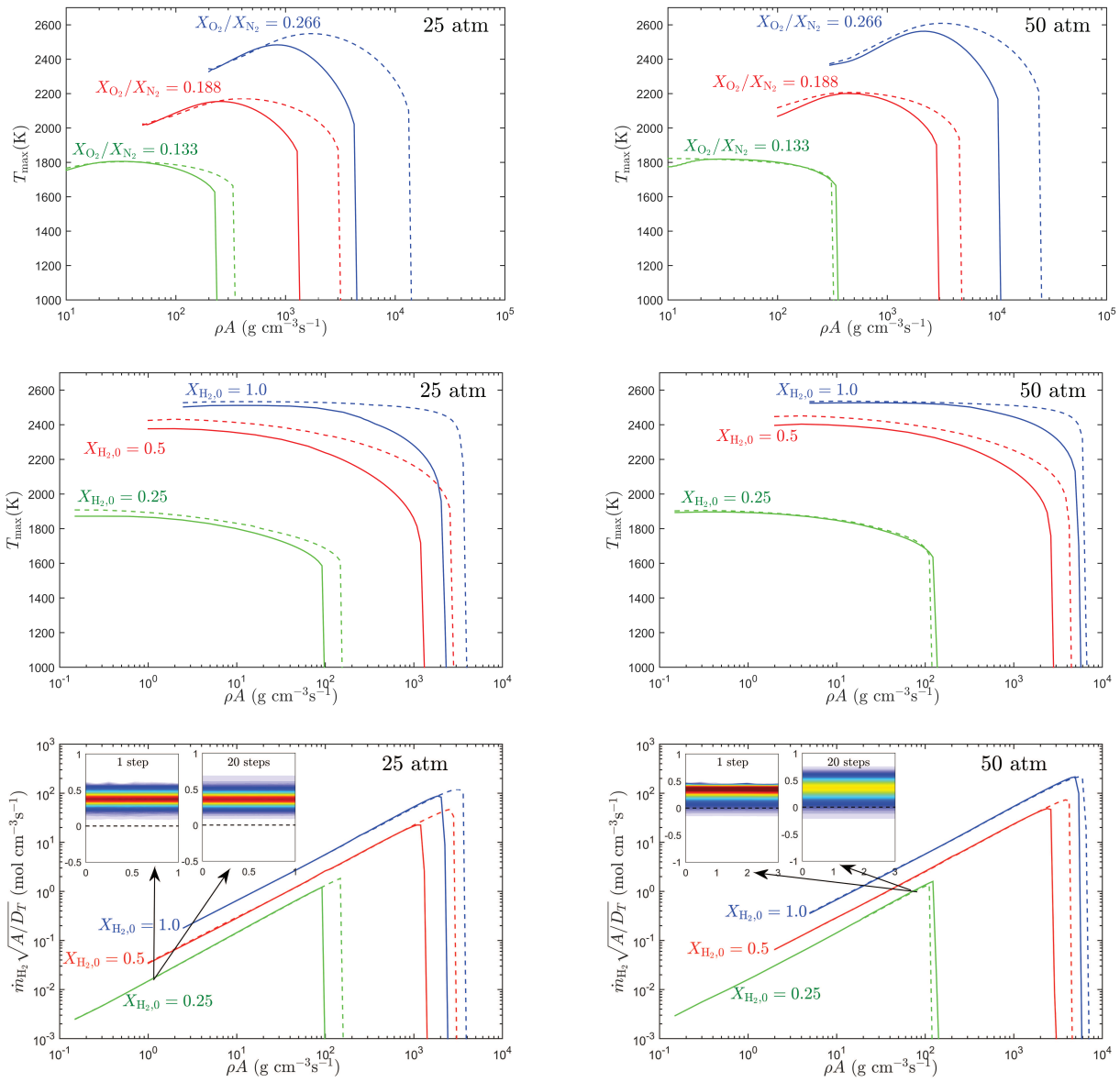

Figure 4: Results of twin premixed flames (upper plots) and diffusion flames (intermediate and lower plots) in a planar counterflow mixing layer as obtained with detailed chemistry (solid curves) and one-step reduced chemistry (dashed curves) for $p = 25$ atm and $p = 50$ atm. The upper plots give the variation with strain rate of the peak temperature in twin-premixed-flames configurations corresponding to H_2-O_2-N_2 mixtures at $T = 300$ K for three different levels of dilution X_{O_2}/X_{N_2}. The intermediate and lower plots give the variation with strain rate of the peak temperature and hydrogen burning rate for a diffusion flame formed between counterflowing streams of air and hydrogen diluted with nitrogen, with $X_{H_2,0}$ representing the hydrogen mole fraction in its feed stream. The color contours in the insets represent the local hydrogen burning rate (mols per unit volume per unit time) of a diffusion flame in a low-strain mixing layer at $p = 25$ atm (left plot) and of a diffusion flame in a high-strain mixing layer near extinction for $p = 50$ atm (right plot).

farther from the crossover temperature, but the general predictive capability remains satisfactory for most purposes, especially away from extinction, where transport rates of chemical intermediates are less pronounced, thereby favoring steady-state approximations [22].

To gain further insight into the effects of strain on the reduced-chemistry performance, insets showing the spatial distribution of fuel burning rate across the one-dimensional diffusion flame with $X_{H_2,0} = 0.25$ are included in the lower panels. The left inset ($p = 25$ atm) depicts the structure of a weakly strained flame, while the right inset ($p = 50$ atm) represents a nearly extinguished flame. The stagnation plane, marked with a dashed line, separates the air stream, flowing from above, from the fuel stream, with the distance from the stagnation plane scaled with the characteristic mixing-layer thickness D_T/A, where D_T is the thermal diffusivity. For the robust flame depicted on the left inset the agreement between the detailed-chemistry results and the reduced kinetics is remarkably good, indicating that at these low strain rates effects of radical transport remain limited. Near extinction, however, the flame thickness predicted by the one-step kinetics, assuming all radicals to be in steady state, is significantly smaller than that of the detailed-chemistry results. It is interesting that this nonnegligible difference in flame structure, which can be attributed to effects of preferential diffusion of H atoms in the presence of high strain rate [3], does not affect significantly the resulting peak temperature or the burning rate per unit flame area $\dot{m}_{H_2}$, so that for diluted flames the overall predictive capabilities of the reduced kinetics remain largely satisfactory even as extinction is approached.

3.3. Partially premixed fronts

The one-dimensional canonical flows investigated above (i.e. steady planar deflagration and counterflow diffusion flame) are useful in characterizing premixed and nonpremixed combustion, but are not suitable for addressing partially premixed conditions, which often prevail near injectors in gas-turbine combustion chambers. In these region, combustion occurs in the form of triple and edge flames propagating along strained mixing layers at velocities (relative to the local flow) that are comparable to those of laminar premixed flames [23]. These reactive fronts play a fundamental role in the stabilization of the combustion process. There is interest, therefore, in assessing whether the one-step kinetics is able to describe sufficiently accurately the propagation of partially premixed fronts under varying levels of strain. A simple problem that serves to investigate these effects is the reactive front propagating along a mixing layer separating two opposed planar jets of fuel and oxidizer, a canonical configuration used previously in theoretical [24–26], experimental [27–29], and numerical [20, 30] studies.

The variation with strain rate of the resulting propagation velocity U when the oxidizer is air and the fuel is a mixture of H_2 and N_2 with $X_{H_2,0} = 1, 0.5, 0.25$ is shown in Fig. 5 for $p = 25$ atm and $p = 50$ atm. The flow ahead of the front is chemically frozen, so that the air mixes with the fuel to generate a mixing layer, across which the composition varies from fuel-rich to fuel-lean conditions, creating the partially premixed conditions encountered by the triple flame, which leaves behind a diffusion flame that eventually develops into the one-dimensional solution described earlier in Fig. 4. For weakly strained configurations with small values of A the mixing layer is much thicker than the front thickness, and a tribrachial

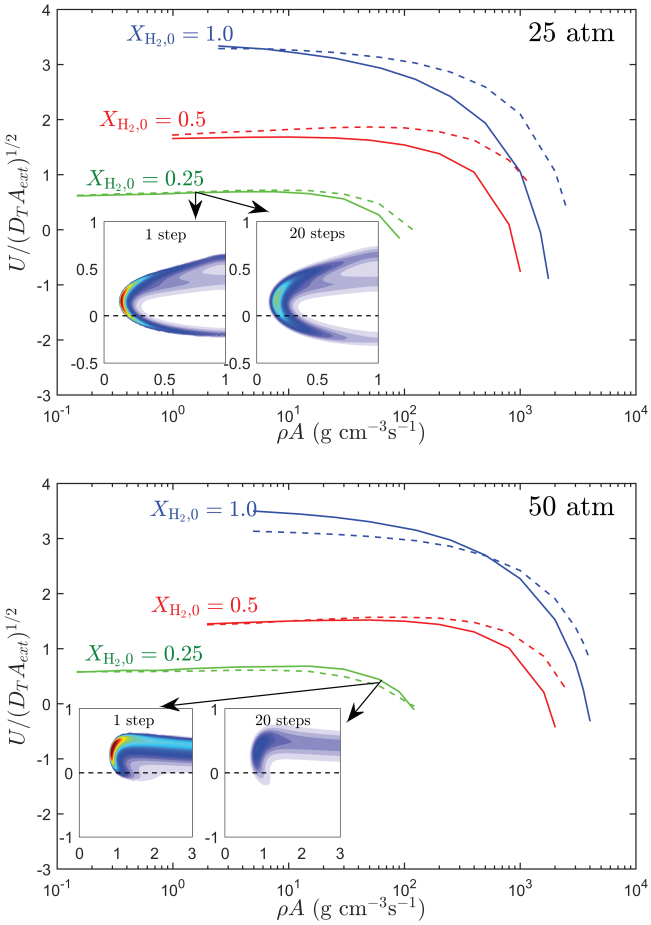

Figure 5: The variation with strain of the velocity U of a triple flame propagating along a two-dimensional mixing layer separating counterflowing streams of air and hydrogen diluted with nitrogen, with $X_{H_2,0}$ representing the hydrogen mole fraction in its feed stream. The velocity is scaled with $(D_T A_{ext})^{1/2}$, where D_T and A_{ext} represent, the thermal diffusivity and the extinction strain rate, respectively, the latter evaluated from the detailed-chemistry computations of Fig. 4. The color contours in the insets represent the local hydrogen burning rate (mols per unit volume per unit time) of an advancing front in a low-strain mixing layer at $p = 25$ atm (upper plot) and of a retreating front near extinction for $p = 50$ atm (lower plot).

structure emerges, including distinct lean and rich branches and a trailing diffusion flame originating from the stoichiometric point. A representative flame is shown in the inset of the upper figure, which shows contours of local fuel burning rate obtained with the detailed and reduced chemistry for the conditions of strain considered earlier in the diffusion-flame computations shown in the left inset of Fig. 4. As can be seen, although for these strain conditions reduced-chemistry fuel-consumption-rate departures are found near the triple point, where the reduced-chemistry results exhibit peak burning rates that are significantly higher than those predicted with the detailed chemistry, which spreads the reactions over larger volumes through radical diffusion. These differences, which likely arise from the high curvature of the front near the triple point, are consistent with previous numerical computations [3], which have shown how flame curvature promotes preferential diffusion of H atoms into pockets of reactants, thereby increasing overall consumption rates by spreading the chemistry over larger volumes (although locally decreasing peak reaction rates).

The propagation speed decreases for increasing strain rates, as the front loses its tribrachial structure to become an edge flame, eventually transitioning to a retreating front with negative U, which extinguishes as the strain rate A reaches the critical value A_{ext} predicted earlier in the computations of Fig. 4. The inset in the lower plot of Fig. 5 shows the structure of one of these near-extinction retreating flames. It is seen that the structure of the edge flame predicted with the one-step kinetics is quite different from that computed with detailed chemistry, in that the latter exhibits a larger thickness resulting from curvature and strain promoting preferential radical diffusion, which is necessarily absent in the reduced-chemistry model, which assumes all radicals to maintain steady state. It is of interest in connection with the predictive capability of the reduced kinetics that the local departures in flame structure illustrated in the insets do not affect significantly the resulting propagation velocity, which for this dilution is almost identical for the two chemistry models, as seen in the green curves.

In view of the curves depicted in Fig. 5, it can be concluded that the one-step kinetics provides a sufficiently accurate description with regards to the propagation speed of partially premixed fronts. The agreement is extremely good for $X_{\mathrm{H}_2,0} = 0.25$, especially at $p = 50$ atm, when the difference $T_{max} - T_c$ takes values on the order of 500 K. Despite the observed reduced accuracy at lower pressure and larger values of $X_{\mathrm{H}_2,0}$, it is remarkable that, even for undiluted fuel feed at $p = 25$ atm, when the difference $T_{max} - T_c$ is on the order of 1000 K, the one-step description still behaves reasonably well, thereby giving additional confidence on the predictive capabilities of the reduced kinetics.

4. Concluding remarks

Replacing the available detailed mechanisms of twenty or more steps by a one-step mechanism can be quite beneficial in computational investigations of hydrogen gas-turbine combustion, provided that the one-step mechanism delivers sufficient accuracy for the chemical kinetics. It may be seen from the results reported herein that, by restricting attention to the combustor pressures, temperatures, and mixture compositions commonly encountered in gas turbines, not only premixed laminar flame temperatures and burning velocities, but also

peak temperatures in strained twin-flame configurations, counterflow diffusion-flame peak temperatures, burning rates, and extinction conditions, and rates of advancement or retreat of partially premixed triple or edge flames, all are predicted with errors at most of the order of ten percent, by the one-step mechanism derived in the present work. This mechanism therefore is likely to be useful in future computational and theoretical investigations.

In the one-step description, transport properties appear for the species O_2, H_2, and H_2O. Effects of preferential diffusion of H_2, found to be important for gas turbines in a previous DNS investigation [3], therefore can readily be accounted for when the present mechanism is employed. It was also found [3] that preferential diffusion of H atoms into pockets of reactants at the trailing edges of turbulent premixed hydrogen flames (a process not compatible with the present chemical-kinetic description since transport properties of steady-state species do not appear) is important in accelerating their rate of final burnout. This aspect of the turbulent combustion therefore is lost with the present chemistry, but that is not likely to affect the predicted overall rate of turbulent flame propagation significantly. This observation is illustrative of the fact the the utility of any reduced-chemistry description such as this is restricted in the range of purposes for which it can be employed, and it cannot, for example, be used to address detailed chemical-kinetic questions that depend on departures from the steady states employed. Such questions, however, are not at the core of most practical investigations, whence the present results may find wide utility.

The results of strained premixed flames shown in the top plots of Fig. 4 reflect expected preferential diffusion effects. Additional computations should assess associated Markstein lengths to further investigate the ability of the reduced kinetics to predict burning-rate dependences on strain rate.

Future work should address limitations of the current results associated with the starting skeletal mechanism used in the description. Addition of H_2O_2 chemistry would be needed to enable predictions of high-pressure flame propagation to be made at temperatures below crossover. Also, consideration of the initiation reaction $H_2+O_2 \stackrel{6b}{\rightarrow} HO_2+H$ is necessary for addressing any branched-chain autoignition process that begins in mixtures devoid of radicals, thereby preventing systematically derived one-step approximations from being applicable to gas-turbine autoignition and motivating further investigations of two-step approximations.

Future research along the present lines that would be relevant for gas-turbine applications would be to extend the one-step hydrogen description to include effects of the chemistry of other fuel constituents expected in the applications, such as methane and ammonia. Since the hydrogen chemistry is comparatively rapid, it should dominate unless the hydrogen content is very small, and other fuels are likely to slow the chemistry, providing retarding mechanisms that may be described by adding a small number of reduced-chemistry steps derived through appropriate additional steady-state approximations. Although these classical asymptotic methods seem currently perhaps to be out of vogue, being supplanted by automatic programs devoid of physical or chemical insights, they appear to us to still have a great deal to offer, not only in improving understanding but also in facilitating computation.

5. Declaration of Competing Interest

The authors declare that they have no known competing financial interests or personal relationships that could have appeared to influence the work reported in this paper.

6. Acknowledgment

We would like to thank two anonymous reviewers whose extensive comments led to significant improvements in our presentation. This work was supported by the US AFOSR Grant No. FA9550-20-0431. The work of J.C. was supported by the Spanish MCIN/AEI/10.13039/501100011033 and by the "European Union NextGenerationEU/PRTR" through grant # TED2021-129446B-C43. The work of D.F.G. was funded by project #PID2019-108592RB-C42/AEI/10.13039/501100011033.

[1] A. Dreizler, H. Pitsch, V. Scherer, C. Schultz, J. Janicka, The role of combustion science and technology in low and zero impact energy transformation processes, Appl. Energy Combust. Sci. 7 (2021) 100040.
[2] M. R. Bothien, A. Ciani, J. P. Wood, F. G, Toward decarbonized power generation with gas turbines by using sequential combustion for burning hydrogen, J. Eng. Gas Turbines Power 141 (2019) 121013.
[3] M. Reith, A. Gruber, F. A. Williams, J. H. Chen, Enhanced burning rates in hydrogen-enriched turbulent premixed flames by diffusion of molecular and atomic hydrogen, Combust. Flame 239 (2022) 111740.
[4] T. P. Coffee, A. J. Kotlar, M. S. Miller, The overall reaction concept in premixed, laminar, steady-state flames. I. Stoichiometries, Combust. Flame 54 (1983) 155–169.
[5] V. N. Gamezo, T. Ogawa, E. S. Oran, Numerical simulations of flame propagation and DDT in obstructed channels filled with hydrogen–air mixture, Proc. Combust. Inst. 31 (2007) 2463–2471.
[6] B. Wang, W. Wei, S. Ma, G. Wei, Construction of one-step H_2/O_2 reaction mechanism for predicting ignition and its application in simulation of supersonic combustion, Int. J. Hydrog. Energy 41 (2016) 19191–19206.
[7] A. L. Sánchez, F. A. Williams, Recent advances in understanding of flammability characteristics of hydrogen, Prog. Energy Combust. Sci. 41 (2014) 1–55.
[8] F. Mauss, N. Peters, B. Rogg, F. Williams, Reduced kinetic mechanisms for premixed hydrogen flames, in: Reduced kinetic mechanisms for applications in combustion systems, Springer, 1993, pp. 29–43.
[9] P. Boivin, A. L. Sánchez, F. A. Williams, Four-step and three-step systematically reduced chemistry for wide-range H_2–air combustion problems, Combust. Flame 160 (2013) 76–82.
[10] A. L. Sánchez, A. Liñán, F. A. Williams, Chain-branching explosions in mixing layers, SIAM J. Appl. Math. 59 (1999) 1335–1355.
[11] K. Gkagkas, R. Lindstedt, The impact of reduced chemistry on auto-ignition of H_2 in turbulent flows, Combust. Th. Model. 13 (2009) 607–643.
[12] D. Fernández-Galisteo, A. Weiss, A. L. Sánchez, F. A. Williams, A one-step reduced mechanism for near-limit hydrogen combustion with general stoichiometry, Combust. Flame 208 (2019) 1–4.
[13] A. L. Sánchez, F. A. Williams, Corrigendum to "recent advances in understanding of flammability characteristics of hydrogen" [Prog. Energy Combust. Sci. 41 (2014) 1–55], Prog. Energy Combust. Sci. 54 (2016) 93–94.
[14] A. L. Sánchez, J. Carpio, F. A. Williams, Unexpected performance of systematically derived one-step chemistry in describing rich hydrogen-air pulsating flames, Combust. Flame 241 (2022) 112068.
[15] D. Fernández-Galisteo, A. L. Sánchez, A. Liñán, F. A. Williams, One-step reduced kinetics for lean hydrogen–air deflagration, Combust. Flame 156 (2009) 985–996.
[16] D. Fernández-Galisteo, A. L. Sánchez, , A. Liñán, F. A. Williams, The hydrogen–air burning rate near the lean flammability limit, Combust. Theory Model. 13 (2009) 741–761.
[17] The San Diego Mechanism: Chemical-Kinetic Mechanisms for Combustion Applications, https://web.eng.ucsd.edu/mae/groups/combustion/mechanism.html, version: 2016-12-14 (2016).

[18] R. J. Kee, G. Dixon-Lewis, J. Warnatz, M. E. Coltrin, J. A. Miller, A Fortran computer code package for the evaluation of gas-phase multicomponent transport properties, Tech. Rep. SAND86-8246, Sandia Labs., Livermore, CA (United States) (1986).
[19] P. H. Paul, DRFM: A new package for the evaluation of gas-phase transport properties, Tech. rep., Sandia Labs., Livermore, CA (United States) (1997).
[20] J. Carpio, P. Rajamanickam, A. L. Sánchez, F. A. Williams, Near-limit H_2-O_2-N_2 combustion in nonpremixed counterflow mixing layers, Combust. Flame 216 (2020) 426–438.
[21] P. A. Libby, A. Liñán, F. A. Williams, Strained premixed laminar flames with nonunity lewis numbers, Combust. Sci. Technol. 34 (1983) 257–293.
[22] A. D. Weiss, A. L. Sánchez, F. A. Williams, Accuracies of reduced mechanisms for predicting acoustic combustion instabilities, Combust. Flame 209 (2019) 405–407.
[23] A. Linán, M. Vera, A. L. Sánchez, Ignition, liftoff, and extinction of gaseous diffusion flames, Annu. Rev. Fluid Mech. 47 (2015) 293–314.
[24] J. Daou, A. Liñán, The role of unequal diffusivities in ignition and extinction fronts in strained mixing layers, Combust. Theory Model. 2 (1998) 449–477.
[25] J. Daou, A. Liñán, Triple flames in mixing layers with nonunity Lewis numbers, Symp. (Int.) Combust. 27 (1998) 667–674.
[26] P. Rajamanickam, W. Coenen, A. L. Sánchez, F. A. Williams, Influences of stoichiometry on steadily propagating triple flames in counterflows, Proc. Combust. Inst. 37 (2019) 1971–1977.
[27] M. S. Cha, P. D. Ronney, Propagation rates of nonpremixed edge flames, Combust. Flame 146 (2006) 312–328.
[28] H. Song, P. Wang, R. S. Boles, D. Matinyan, H. Prahanphap, J. Piotrowicz, P. D. Ronney, Effects of mixture fraction on edge-flame propagation speeds, Proc. Combust. Inst. 36 (2017) 1403–1409.
[29] Z. Zhou, S. S. Applebaum, P. D. Ronney, Effect of stoichiometric mixture fraction on nonpremixed H_2-O_2-N_2 edge-flames, Proc. Combust. Inst. 37 (2019) 1989–1996.
[30] F. Al-Malki, P. Ronney, The combined effects of chemical reaction order and stoichiometry on non-premixed edge flames, Combust. Theory Model. 25 (2021) 1195–1210.